DOI: 10.1002/chem.200500971

Characterization and Catalytic-Hydrogenation Behavior of SiO_2-Embedded Nanoscopic Pd, Au, and Pd–Au Alloy Colloids

Vasile I. Pârvulescu,*[a] Viorica Pârvulescu,[b] Uwe Endruschat,[c] George Filoti,[d] Friedrich E. Wagner,[d] Christian Kübel,[e] and Ryan Richards[f]

Dedicated to Professor Helmut Bonnemann on the occasion of his 65th birthday

Abstract: Colloids embedded in a silica sol–gel matrix were prepared by using fully alloyed Pd–Au colloids, and pure Pd and Au colloids stabilized with tetraalkylammonium bromide following a modified sol–gel procedure with tetrahydrofuran (THF) as the solvent. Tetraethoxysilicate (TEOS) was used as the precursor for the silica support. The molar composition of the sol was TEOS/THF/H_2O/HCl = 1:3.5:4:0.05 for the bimetallic Pd–Au and TEOS/THF/H_2O/HCl = 1:4.5:4:0.02 for Pd and Au monometallic systems. After refluxing, the colloid was added as a 4.5 wt % solution in THF for Pd–Au, 10.2 wt % solution in THF for Pd and 8.4 wt % solution in THF for Au at room temperature. The gelation was carried out with vigorous stirring (4 days) under an Ar atmosphere. Following these procedures, bimetallic Pd–Au–SiO_2 catalysts with 0.6 and 1 wt % metal, and monometallic Pd– and Au–SiO_2 catalysts with 1 wt % metal were prepared. These materials were further treated following four different routes: 1) by simple drying, 2) in which the dried catalysts were calcined in air at 723 K and then reduced at the same temperature, 3) in which they were directly reduced in hydrogen at 723 K, and 4) in which the surfactant was extracted using an ethanol–heptane azeotropic mixture. The catalysts were characterized by nitrogen adsorption–desorption isotherms at 77 K, H_2 chemisorption measurements, solid-state ^1H, ^{13}C, ^{29}Si-CP/MAS-NMR spectroscopy, powder X-ray diffraction (XRD), small angle X-ray scattering (SAXS), X-ray photoelectron spectroscopy (XPS), transmission electron microscopy (TEM), and ^{197}Au Mössbauer spectroscopy. The physical characterization by a combination of these techniques has shown that the size and the structural characteristics of the Pd–Au colloid precursor are preserved when embedded in an SiO_2 matrix. Catalytic tests were carried out in selective hydrogenation of 3-hexyn-1-ol, cinnamaldehyde, and styrene. These data showed evidence that alloying Pd with Au in bimetallic colloids leads to enhanced activity and most importantly to improved selectivity. Also, the combination of the two metals resulted in catalysts that were very stable against poisoning, as was evidenced for the hydrogenation of styrene in the presence of thiophene.

Keywords: alloys · colloids · hydrogenation · nanostructures · sol–gel processes

[a] Prof. V. I. Pârvulescu
University of Bucharest, Faculty of Chemistry
Department of Chemical Technology and Catalysis
B-dul Regina Elisabeta 4–12
Bucharest 70346 (Romania)
Fax: (+40) 213-159-249
E-mail: v_parvulescu@chem.unibuc.ro

[b] Dr. V. Pârvulescu
Institute of Physical Chemistry of Romanian Academy of Sciences
Splaiul Independentei 202
Bucharest (Romania)

[c] Dr. U. Endruschat
W.C. Heraeus GmbH & Co. KG, Chemicals Division
Heraeusstr. 12–14, 63450 Hanau (Germany)

[d] Dr. G. Filoti, Prof. F. E. Wagner
Technische Universität München, Physics Department E 15
James Franck Strasse 1
85747 Garching bei München (Germany)

[e] Prof. C. Kübel
Fraunhofer Institute for Manufacturing Technology and Applied Materials Science, Wiener Strasse 12
28359 Bremen (Germany)

[f] Prof. R. Richards
School of Engineering and Science
International University Bremen, Campus Ring 8
28759 Bremen (Germany)

Introduction

Supported bimetallic catalysts have elicited a great deal of interest, especially motivated by an observed increase of the selectivity and stability in several catalytic processes of practical importance.[1,2] The element Pd is one of the most investigated in this capacity, but interest has mainly focused towards increasing its activity and stability. Among the numerous metals which were investigated in combination with Pd, Au was found to exhibit a particular influence.[3–12] Gold by itself supported on SiO_2, Al_2O_3, or MgO exhibits rather low catalytic activity.[13] The fact that its activity is lower than that of Group 8 metals was explained by the absence of unpaired d electrons in its electronic structure; this absence prevents Au from chemisorbing dihydrogen or dioxygen at ambient temperature.[14] The increase of the noble-metal activity by adding Pd offered good opportunities to investigate basic principles in catalysis as a function of geometric and electronic effects.[15–17]

Pd–Au catalysts have been demonstrated to be particularly effective in a number of reactions, including hydrogenation of organic compounds,[3,4] production of vinyl acetate,[4–8] liquid-phase oxidation of glyoxal to glyoxalic acid,[8] and hydrodechlorination of chloro- and chlorofluorocarbons.[9–12] The addition of Au has been claimed to improve both the catalytic performance and the stability against deactivation of Pd, as in the case of sulfur. Boitiaux et al. have shown that Pd promoted with Au is a suitable catalyst for selective hydrogenation in the downstream treatment of naphtha cracking, reducing the formation of green oil.[3]

Au and Pd bimetallic nanoparticles, either as alloys or core/shell structures, have received significant attention because of their special catalytic properties. Toshima et al.[18] have described the catalytic activity and analyzed the structure of the poly(*N*-vinyl-2-pyrolidone)-protected Au/Pd bimetallic clusters prepared by simultaneous reduction of $HAuCl_4$ and $PdCl_2$ in the presence of poly(*N*-vinyl-2-pyrolidone). Other groups have reported the formation of Au/Pd bimetallic particles with a palladium-rich shell by a simultaneous alcoholic-reduction method.[19] Successive alcoholic reduction did not give the core/shell-structured products, but instead "cluster-in-cluster" structured products or mixtures of the monometallic particles. Harada et al.[20] and Mizukoshi et al.[21] reported the preparation and structure of Au/Pd bimetallic nanoparticles by sonochemical reduction of gold(III) and palladium(II) ions, Remita et al.[22] used pulse electron-beam irradiated on Au–Pd ion-mixed solutions, while Harpeness and Gedanken[23] used the microwave-assisted polyol method. Wu et al.[24] described the synthesis of Au/Pd bimetallic nanoparticles in reverse micelles of water/sodium bis(2-ethylhexyl)sulfosuccinate (AOT)/isooctane by the coreduction of $HAuCl_4$ and H_2PdCl_4 with hydrazine at 25 °C.

To provide effective catalysts it has been suggested that Au must be intimately mixed with Pd;[24] however, the preparation of a supported homogeneous Pd–Au bimetallic system is a rather complicated problem due to the segregation tendency of these metals.[4] Most reports on bimetallic Pd catalysts refer to systems prepared by means of a co-impregnation of the metal salts on solid supports using an incipient wetness technique followed by calcination.[25–29] However, by using the usual preparation procedures some metal sintering and segregation of the surface is evident.[28,30,31] Reduction at high temperature in molecular dihydrogen and interaction of these metals with the support favor this process.[32] During segregation the more noble metal constitutes the core and the less noble metal the shell of a bilayered cluster. Therefore, among the techniques proposed to prepare supported homogeneous bimetallic Pd–Au catalysts Diamy et al.[33] proposed the afterglow of a dihydrogen microwave plasma (2450 MHz), which contains active species (mainly atomic hydrogen) and which makes it possible to work at a kinetic temperature low enough to avoid the formation of large particles. Deposition of the two metals onto the zeolite support was carried out by successive exchange. However, even the resulting system did not consist of alloyed metals.

However, significantly supported Pd–Au homogeneous alloy structures were prepared by either low[34] or high-temperature procedures.[35] In the low-temperature procedure silica was metallated with $[Au(en)_2]^{3+}$ upon ion exchange. The presence of a Pd–Au alloy together with monometallic species and PdO clusters was reported by Guczi et al. in the case of Pd–Au/TiO_2 and Pd–Au/SiO_2 catalysts.[36,37] Bonarowska et al. reported a new procedure for the preparation of homogeneous Pd–Au bimetallic catalysts.[25] These authors showed that more readily reducible gold ions might be directly reduced by prereduced Pd species, resulting in intimate contact of both metals. However, a vigorous debate is ongoing as to whether the resulting Pd–Au particles on the support using these preparation techniques are fully alloyed.[25,28] A combined X-ray absorption near-edge structure (XANES) and extended X-ray absorption fine structure (EXAFS) study by Couves and Meeham[38] emphasized these doubts. For the system Pd–Au/MgF_2, Malinowski et al.[11] demonstrated the existence of two Pd–Au solid solutions, Pd/Au 0.81:0.19 and Pd/Au 0.4:0.6, and that not all the metal is reduced.

A further problem lies in the dispersion of the metal. There is strong evidence that the addition of Au to Pd salts results in a marked decrease of the dispersion of the bimetallic catalyst systems.[31] An innovative procedure to prepare bimetallic catalysts containing Au was first proposed by Turkevich et al.[39,40] They suggested that preformed colloids can be embedded in an oxidic matrix leading to very active and stable systems. Afterwards, numerous reports about the synthesis of Pd–Au bimetallic colloids using different reductants and in the presence of different stabilizer ligands appeared in the literature.[41–46] By using this approach, highly dispersed bimetallic catalyst precursors could be prepared. Following the so-called "precursor concept",[47] such pre-prepared nanometals, in which the particle size distribution, composition, and structure is rather well defined, may be deposited on various supports giving a new type of heterogeneous, bimetallic catalyst.[47–49]

The incorporation of preformed ligand-stabilized metal clusters and colloids into heterogeneous catalyst systems is currently of interest. Most of the studies have been done using polymer- or dendrimer-stabilized metal colloids and several ways have been proposed to solve this problem.[50–60] Organic polymers are not very stable at high temperature and the catalytic reaction in solution may be accompanied by some swelling, which can cause mass-transfer diffusion problems. Therefore the use of inorganic supports appears to be more suitable.

The incorporation of metal colloids into inorganic matrices has also been reported in the literature.[61–63] Sol–gel has also been shown as an effective technique to embed nanoscale mono- and bimetallic noble metals.[64–66] Yu et al. reported[67] that metal particles of tailored size (3–5 nm) and composition prepared by means of inverse microemulsion were encapsulated by ultrathin coatings (<2.5 nm) of inorganic porous SiO_2 aerogels covered with surface OH groups. These composite materials were then anchored to conventional solid supports (alumina, carbon) upon mixing. More recently, Crooks and co-workers reported synthesis of TiO_2-supported Pd–Au bimetallic nanoparticle catalysts prepared using dendrimer-encapsulated nanoparticles. For such purposes the dendrimer-encapsulated nanoparticles were embedded in TiO_2 by using a polymeric sol–gel procedure with $Ti(OiPr)_4$ as a precursor.[68] Another attempt to entrap aqueous monometallic nanoparticles on the surface of micrometer-sized zeolite particles functionalized with amine groups was proposed by Mandal et al,[69] who bound Pt and Pd nanoparticles at high surface coverage on 3-aminopropyltrimethoxysilane (APTS)-functionalized Na–Y zeolites. All these data confirm that the incorporation of bimetallic colloids is a complicated problem, because the components may interact differently with the support. In a previous communication, we reported the preparation of a heterogeneous Pd–Au catalyst by embedding pre-prepared tetraalkylammonium-stabilized Pd–Au alloy particles in a solid SiO_2 matrix following a modified sol–gel process.[70] Encapsulation of nanometer-sized metals in solid matrices was also investigated. Ichikawa used both micro- and mesoporous silica supports to prepare nanowire metals. However, such a procedure limits the catalytic performance of the resulting composites, since most of the pores are blocked. Also, for bimetallic catalysts the control of alloying inside the pores is rather small.[71–73]

A new approach has been proposed by the group of Schmid. To preserve the organization of the colloids inside the pores these authors proposed functionalization of the interior pore surface by reacting OH groups with alkoxylsilyl-substituted, short diphosphane ligands.[74–76] However, these can immobilize only very small clusters, which are then rather sensitive to the reaction media, mostly to leaching. In addition, this technique is more versatile for monometallic clusters.

The size of the metallic ensembles is another critical issue related to supported bimetallic catalysts.[4] The use of impregnation techniques evidently leads to a dispersion in the metal–particle size. The "precursor concept",[47] however, eliminates this hindrance. Therefore, the incorporation of colloids with well-defined particle size may yield additional information to highlight the effect of the ensemble size in heterogeneous catalysis. Further structural characterization of the supported bimetallic catalysts and especially the homogeneity of these catalysts is a complicated task.

The aim of this work is to present evidence about the integrity of SiO_2-embedded Pd, Au, and Pd–Au highly alloyed colloids prepared by sol–gel embedding of presynthesized colloids and their performances in the hydrogenation of several substrates: cinnamaldehyde, 3-hexyn-1-ol, and styrene. The catalysts were characterized by adsorption–desorption isotherms of nitrogen at 77 K, H_2 chemisorption, XRD, SAXS, ^{197}Au Mössbauer spectroscopy, and XPS.

Results

Catalysts preparation: Scheme 1 depicts the synthesis of SiO_2-embedded nanoscopic Pd, Au, and Pd-Au alloy colloids. After the gelation has been fulfilled the materials were treated following the four routes D, C, R, and E described in Scheme 1. Actually, in addition to the chemical composition of the colloid and its loading, these treatments further differentiate the investigated catalysts. Therefore, further characterization and catalytic-behavior discussions

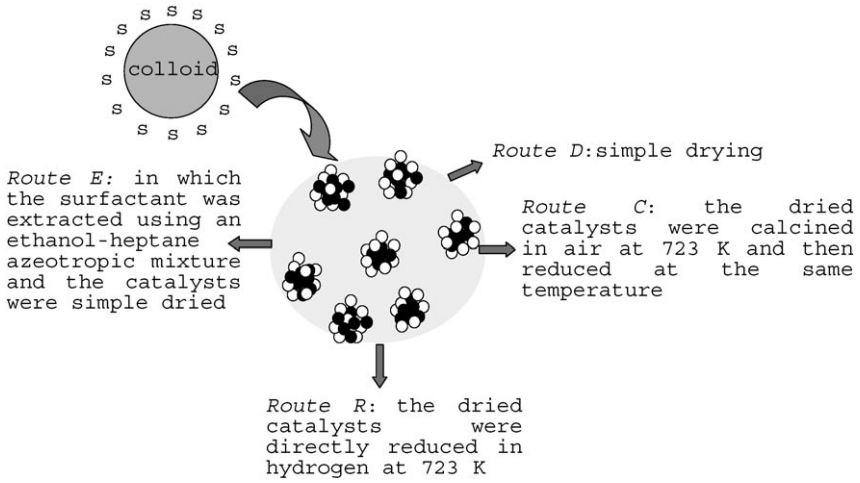

Scheme 1. Synthesis of SiO_2-embedded nanoscopic Pd, Au, and Pd–Au alloy colloids. Routes C, D, E, R; TEOS/THF/H_2O/HCl = 1:3.5:4:0.05 for Pd–Au; TEOS/THF/H_2O/HCl = 1:4.5:4:0.02 for Pd and Au.

will refer mainly to these treatments, by nominating catalysts belonging to one of these groups (D, C, R, or E).

Textural characterization: Thermal activation (723 K) of such hybrid materials resulted in a porous texture with a rather narrow pore diameter in the region of the mesoporous materials. Similar data were obtained for dried samples after they were treated following a procedure proposed by Hitz and Prins.[77] For all the samples the Brunauer–Emmett–Teller (BET) surface areas of series D were higher than those of series C and R. Extraction of the stabilizer compound (sample E) led to even higher surface areas. Such behavior can be correlated to the space occupied by the stabilizer compound (upon extraction of the stabilizer this space may result in additional surface area in the case of sample E) and the amount of carbonaceous species formed by thermal decomposition and insufficiently removed (sample D). These data are compiled in Table 1.

Table 1. Textural characteristics of SiO_2-embedded colloids.

Catalyst	Pd/Au ratio	BET surface area [m^2g^{-1}]	Average pore size [nm]
C-0.6 % (Pd-Au)-SiO_2	52 : 48	267	16.6
R-0.6 % (Pd-Au)-SiO_2	52 : 48	97	17.3
D-0.6 % (Pd-Au)-SiO_2	52 : 48	304	16.1
E-0.6 % (Pd-Au)-SiO_2	52 : 48	323	16.2
C-1 % (Pd-Au)-SiO_2	52 : 48	193	18.8
R-1 % (Pd-Au)-SiO_2	52 : 48	78	20.2
D-1 % (Pd-Au)-SiO_2	52 : 48	231	18.1
E-1 % (Pd-Au)-SiO_2	52 : 48	244	18.1
C-1 % (Pd)-SiO_2	–	261	23.0
R-1 % (Pd)-SiO_2	–	87	25.2
D-1 % (Pd)-SiO_2	–	298	22.6
E-1 % (Pd)-SiO_2	–	319	22.7
C-1 % (Au)-SiO_2	–	201	22.8
R-1 % (Au)-SiO_2	–	56	24.0
D-1 % (Au)-SiO_2	–	259	22.1
E-1 % (Au)-SiO_2	–	273	22.1

SAXS investigation of these materials indicated that pores were randomly distributed. No pore organization has been detected.

Hydrogen chemisorption data: Table 2 contains the H_2 chemisorption data. The hydrogen uptake on Au colloids was very small, in agreement with the literature data for Au.[31] The presence of Au in Pd–Au colloids also led to a decrease of the hydrogen uptake, relative to Pd-containing samples.

Table 2. Hydrogen chemisorption data for SiO_2-embedded catalysts.

Catalyst	Chemisorbed H_2 uptake [cm^3g^{-1}]	Dispersion [%]	SM[a] [$m^2g^{-1}_{sample}$]	SM[a] [$m^2g^{-1}_{sample}$]
C-0.6 % (Pd-Au)-SiO_2	0.1201	12.2	0.25	25.4
R-0.6 % (Pd-Au)-SiO_2	0.0887	9.0	0.19	18.7
D-0.6 % (Pd-Au)-SiO_2	0.1261	12.8	0.27	26.7
E-0.6 % (Pd-Au)-SiO_2	0.1279	13.1	0.28	27.7
C-1 % (Pd-Au)-SiO_2	0.1989	12.1	0.42	42.1
R-1 % (Pd-Au)-SiO_2	0.1661	10.1	0.35	35.1
D-1 % (Pd-Au)-SiO_2	0.2087	12.7	0.44	44.1
E-1 % (Pd-Au)-SiO_2	0.2148	13.1	0.45	45.3
C-1 % (Pd)-SiO_2	0.2233	10.6	0.47	47.2
R-1 % (Pd)-SiO_2	0.2145	10.1	0.45	45.3
D-1 % (Pd)-SiO_2	0.2367	11.2	0.50	50.0
E-1 % (Pd)-SiO_2	0.2536	12.0	0.55	55.6
C-1 % (Au)-SiO_2	0.0840	7.4	0.24	24.8
R-1 % (Au)-SiO_2	0.0734	6.4	0.21	21.5
D-1 % (Au)-SiO_2	0.0865	7.6	0.25	25.6
E-1 % (Au)-SiO_2	0.0869	7.6	0.25	25.6

[a] SM = Metallic surface area.

For each series of catalyst the hydrogen uptake was increased in the order: D ~ E > C > R. During the direct reduction of the catalysts, part of the protector template was decomposed to coke which hindered hydrogen chemisorption, while the samples in which the template was extracted exhibited higher hydrogen uptake than the calcined or directly reduced samples.

Dispersion of the embedded metal colloids was also rather low. The bimetallic-embedded colloids with 0.6 and 1.0 wt % metal exhibited almost the same dispersion, which proves the reproducibility of the preparation procedure. Dispersion of the monometallic Pd colloid in the silica-gel matrix was found to be lower than in the case of the bimetallic Pd–Au colloid in the same matrix. For the same metal loading, the Au-containing silica-gel matrix exhibited the lowest dispersion.

X-ray diffraction (XRD): XRD patterns of the embedded Au, Pd, and Pd–Au colloids show an intensity distribution corresponding to silica and to metallic or bimetallic species. Figure 1 presents the patterns for the calcined and reduced samples (i.e., samples D). With the exception of the reflection lines of silica, these patterns are identical to those recorded for stabilized colloids. An intense diffraction peak at $2\theta = 22°$ originates from calcined SiO_2, showing that the support is not totally amorphous. All peaks in the pattern recorded for the bimetallic system containing 1.0 wt % Pd–Au in SiO_2 correspond to a bimetallic Pd–Au alloy, and no peaks can be attributed to the presence of monometallic Au or Pd species. A peak-broadening analysis was performed on the basis of full width at half maximum (FWHM) values obtained from peak fitting by using a pseudo-Voigt, peak-shape function. The instrument line broadening was obtained by using a standard Si sample. The result indicates a particle size of about 4.9 nm both for the Pd–Au and the Au system, whereas the particles in the pure Pd system appear to be larger (ca. 5.6 nm). From the lattice-parameter calculation for the Au colloid (cubic $Fm3m$, $a = 4.074$ Å), Pd colloid

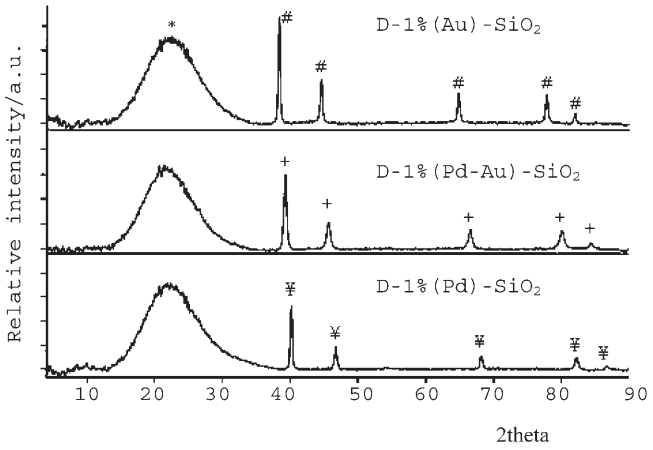

Figure 1. XRD patterns of the D catalyst series: (*) SiO_2; (¥) Pd; (#) Au; (+) Pd–Au.

($a = 3.886$ Å), and Pd–Au alloy colloid ($a = 3.976$ Å), a 52 wt% Au and 48 wt% Pd composition of the Pd–Au system has been concluded.

Embedding of the colloids, calcining followed by reduction with hydrogen, direct reduction with hydrogen, or extraction of the stabilizer compound from the embedded catalysts did not produce any change in the position or intensity of the reflection lines assigned to the metallic colloids as compared with pure colloids.

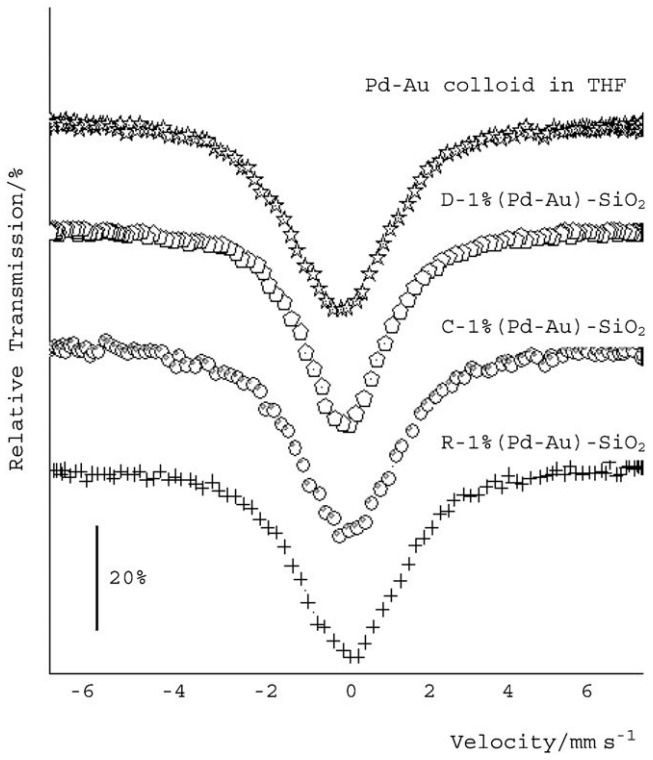

Figure 2. Mössbauer spectra of Au–Pd samples.

Mössbauer spectroscopy: Figure 2 shows typical Mossbauer spectra recorded for the investigated catalysts. For the noncalcined, embedded Pd–Au colloids, the lines (Figure 2 and Table 3) are noticeable, but are not much broader than those of the equivalent alloys obtained by traditional methods. This represents a good indication that they are macroscopically homogeneous. Therefore, one can rule out any surface segregation of the component elements or broadening due to small particle effects, most probably because the colloids are rather small (ca. 3.9 nm, as derived from XRD measurements). Treating the catalysts in hydrogen at 723 K (R series, Figure 2 and Table 3) produced an enlargement of the line, this enlargement is comparable with values obtained for nonembedded colloids. This effect apparently could be attributed to a segregation tendency into more Pd- and Au-rich fractions, perhaps with one metal accumulating on the surface. However, the two metals did not become separated after heating. Segregation would lead to Au being surrounded by more Au and less Pd, which would give rise to smaller mean isomer shifts. Therefore, it appears that this enlargement is caused by a change in the colloid–support interaction. Such a supposition is also supported by the spectra recorded for the catalysts with 0.6% (Pd–Au) (Table 3), in which more metal is supposed to be directly interacting with silica. Simple calcination (more evident for the catalyst in series C with 1% (Pd–Au)) is less influenced by this interaction than the reduced catalysts.

Table 3. Mössbauer results for samples of Au and Au–Pd Alloy colloids (embedded in silica or unsupported) and for rolled foils of Au and Au–Pd alloys used as reference materials.[a]

Sample	IS [mm s^{-1}]	σ [mm s^{-1}]	A_{tot}	d [mg cm^{-2}]
D-1% (Au)-SiO_2	−1.227 (7)	0.446 (16)	0.147 (1)	1974
R-1% (Au)-SiO_2	−1.224 (5)	0.258 (17)	0.140 (1)	851
C-1% (Au)-SiO_2	−1.268 (8)	0.295 (25)	0.112 (1)	975
D-1% (Pd-Au)-SiO_2	−0.015 (7)	0.400 (17)	0.257 (2)	1768
R-1% (Pd-Au)-SiO_2	0.048 (12)	0.680 (19)	0.123 (1)	842
C-1% (Pd-Au)-SiO_2	−0.038 (5)	0.404 (10)	0.198 (1)	1432
D-0.6% (Pd-Au)-SiO_2	0.182 (6)	0.466 (13)	0.166 (1)	1694
R-0.6% (Pd-Au)-SiO_2	0.180 (11)	0.473 (18)	0.160 (1)	1657
C-0.6% (Pd-Au)-SiO_2	0.163 (8)	0.430 (19)	0.158 (1)	1638
Au-Pd colloid in THF	−0.118 (7)	0.707 (11)	0.179 (1)	—
Au	−1.232 (4)	0.0 fixed	0.644 (3)	100
$Au_{0.60}$ $Pd_{0.40}$ as rolled	−0.465 (3)	0.386 (8)	0.267 (1)	16.0
$Au_{0.60}$ $Pd_{0.40}$ annealed	−0.410 (2)	0.279 (7)	0.439 (1)	16.0
$Au_{0.50}$ $Pd_{0.50}$ as rolled	−0.275 (2)	0.378 (5)	0.280 (1)	14.0
$Au_{0.50}$ $Pd_{0.50}$ annealed	−0.207 (2)	0.295 (7)	0.403 (1)	28.9
$Au_{0.40}$ $Pd_{0.60}$ as rolled	−0.013 (4)	0.403 (10)	0.202 (1)	16.0
$Au_{0.40}$ $Pd_{0.60}$ annealed	0.054 (3)	0.299 (7)	0.483 (1)	28.9
$Au_{0.10}$ $Pd_{0.90}$ as rolled	0.802 (4)	0.197 (19)	0.562 (2)	90[b]
$Au_{0.05}$ $Pd_{0.95}$ as rolled	0.905 (5)	0.158 (25)	0.157 (1)	90[b]
$Au_{0.03}$ $Pd_{0.97}$ as rolled	0.916 (7)	0.143 (40)	0.074 (1)	40[b]

[a] IS: Isomer shift with respect to a Au:Pd source; σ: width of the Gaussian distribution of line positions; A_{tot}: total area under the absorption line; d: absorber thickness. Last digit errors are given in parentheses; these errors are the statistical ones only. Annealed samples were treated in H_2 in similar conditions with the R catalyst series. [b] Thickness given in μm.

As mentioned above, the nonembedded Pd–Au colloids (Figure 2) measured in frozen THF definitely have a broad-

er line than that of the embedded ones. It could be derived either from the smaller size of particles or from a random distribution of Au and Pd in the investigated colloids.

Mössbauer spectra of pure Au colloids after heating (both in an air and hydrogen atmosphere) give narrower lines that indicate either a cluster shape phenomenon or a colloid agglomeration on annealing.[78–80]

The results obtained for the mean isomer shifts and for the variance of the Gaussian distribution of isomer shifts are given in Table 3 for samples of Au, Au–Pd alloy colloids and for the arc-melted alloys used as reference materials. Electric-quadrupole interactions were not explicitly taken into account in the fitting procedure, but one should keep in mind that they should exist in random alloys, because the distribution of Au and Pd have different radii breaks and perfect local-cubic symmetry. Moreover, in small particles, the cubic symmetry is evidently broken for surface atoms.

No differences have been observed in the Mössbauer spectra between samples D and E.

The as-rolled alloys $Au_{60}Pd_{40}$ to $Au_{40}Pd_{60}$ lie about 0.1 mm s^{-1} below the straight line connecting the data points for pure Au and dilute Au in Pd. Treatment of the rolled alloys in hydrogen at 723 K for 20 h leads to a slight increase in the isomer shift (Table 3). Moreover, the lines become somewhat narrower during this treatment, that is, σ decreases slightly. This indicates that the distribution of Au and Pd in the vicinity of the Au atoms changes during the thermal treatment in the sense that Au is surrounded by somewhat more Pd and fewer Au atoms than Au in the as-rolled foils. The distribution of Au and Pd in the vicinity of Au apparently also becomes narrower.

Comparing the Mössbauer spectra of the embedded Pd–Au colloids with those of the rolled alloys shows that colloids contain lines slightly broader than those of the rolled alloys. This is additional confirmation that they are macroscopically homogeneous and remain intact even after thermal treatment.

Figure 3 shows the isomer shifts as a function of the alloy composition near the $Au_{50}Pd_{50}$ composition. The line in this figure is a straight line connecting the datum point for pure Au with that of dilute alloys of Au in Pd. The data for all Au–Pd colloid samples is plotted at the composition $Au_{50}Pd_{50}$. The isomer shifts for all compositions lie above that for the rolled and thermally treated $Au_{50}Pd_{50}$ alloy by up to 0.25 mm s^{-1}. This can be interpreted in two ways: 1) as a shift arising from small particle effects or 2) as a shift caused by Au in the particles surrounded on average by more than 50% Pd. The obvious explanation for this would be that the colloids contain more than 50% Pd, which is in total concordance with analytical results.

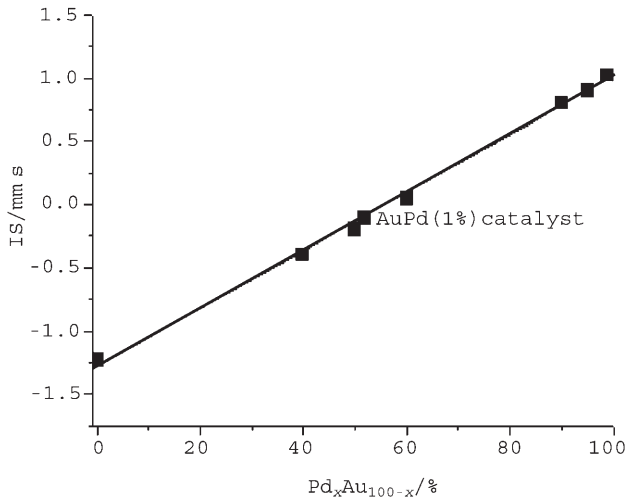

Figure 3. Dependence of the Mössbauer isomer shift on the alloy composition

Heating all these samples (rolled alloys and colloids) resulted in an increase of the isomer shift, which may indicate that indeed the number of Pd atoms in the vicinity of Au increases by heating. However, as was mentioned before, the increase in isomer shifts induced by heating cannot be attributed to segregation. Segregation would lead to Au being surrounded by more Au and less Pd, which in turn would lead to a smaller mean isomer shift. It could only result from a homogenization of the Au–Pd distribution, or from colloid–surface effects like changes of the colloid shape or of the colloid–support interactions.

X-ray photoelectron spectroscopy (XPS): Table 4 contains the XPS results of the investigated catalysts. In all samples the binding energy assigned to Pd and Au species corresponds to Pd^0[81] and Au^0[82] components. Calcination fol-

Table 4. XPS characteristics of the investigated catalysts.

Catalyst	Binding Energy [eV]			XPS Pd/Au ratio	XPS M[a]/Si ratio × 10^3
	Pd3d$_{3/2}$	Au4d$_{3/2}$	Si2p		
C-0.6% (Pd-Au)-SiO$_2$	340.9	353.1	103.6	1.10	3.3
R-0.6% (Pd-Au)-SiO$_2$	340.9	353.0	103.5	1.09	3.2
D-0.6% (Pd-Au)-SiO$_2$	340.8	353.1	103.4	1.12	3.1
E-0.6% (Pd-Au)-SiO$_2$	340.7	353.1	103.6	1.10	3.2
C-1% (Pd-Au)-SiO$_2$	340.9	353.0	103.6	1.11	6.3
R-1% (Pd-Au)-SiO$_2$	340.9	353.0	103.6	1.08	6.2
D-1% (Pd-Au)-SiO$_2$	340.8	353.1	103.5	1.12	6.4
E-1% (Pd-Au)-SiO$_2$	340.8	353.0	103.6	1.14	6.5
C-1% (Pd)-SiO$_2$	340.9	353.1	103.5	1.12	5.3
R-1% (Pd)-SiO$_2$	340.9	353.0	103.6	1.08	5.4
D-1% (Pd)-SiO$_2$	340.8	353.0	103.4	1.09	5.4
E-1% (Pd)-SiO$_2$	340.8	353.0	103.6	1.07	5.1
C-1% (Au)-SiO$_2$	340.9	353.1	103.6	1.11	4.6
R-1% (Au)-SiO$_2$	340.8	353.1	103.5	1.12	4.5
D-1% (Au)-SiO$_2$	340.8	353.0	103.6	1.13	4.4
E-1% (Au)-SiO$_2$	340.7	353.1	103.6	1.12	4.3

[a] M = Pd, Au or (Pd + Au).

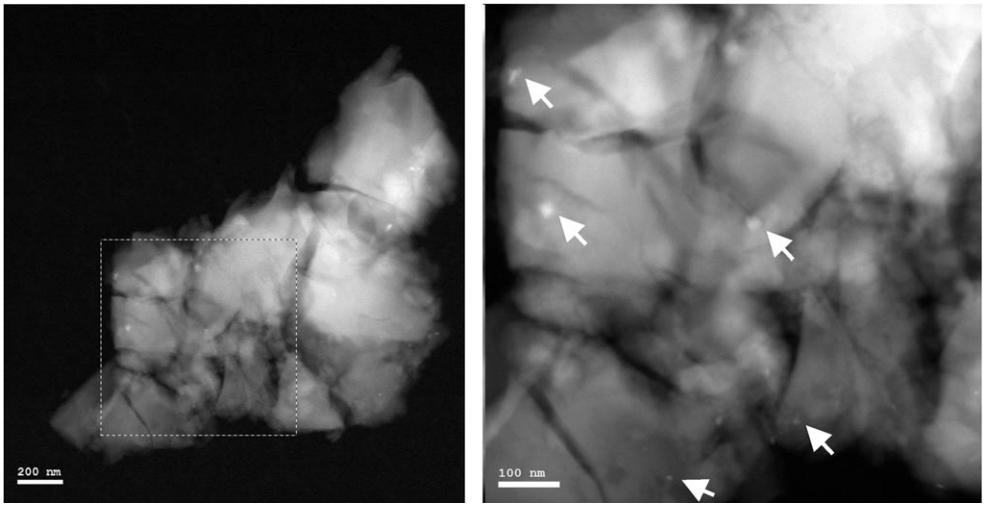

Figure 4. HAADF-STEM overview together with a more detailed image showing the distribution of the Pd and Au particles as bright spots (some of them indicated by arrows) in the SiO_2 matrix. The scalebars represent 200 and 100 nm in the left- and right-hand images, respectively.

lowed by reduction or direct reduction of these samples did not cause any change in the oxidation state of these elements, indicating very good stability of the embedded colloids. The values determined for the Pd/Au ratios, which were indeed in a very narrow interval for all these samples, irrespective of the treatment they were exposed to, are also very important. The ratios given in Table 4 actually correspond to atomic Pd/Au ratios between 53:47 and 52:48, which is the same ratio as that determined by Mössbauer and XRD measurements. The stability of the embedded colloids was also confirmed by the XPS atomic Pd, Au, or (Pd–Au)/Si ratios. The values presented in Table 4 also confirm the fact that different treatments do not affect the colloid integrity and dispersion.

TEM analysis: Grinding the bulk C-1 % Pd–Au/SiO_2 resulted in fragments with a typical diameter of 0.2–2 μm. High-angle annular dark-field scanning transmission electron microscopy (HAADF–STEM) imaging of these fragments revealed the distribution of the Au and Pd nanoparticles as bright spots in the SiO_2 matrix. The size distribution and particle density varied quite a bit throughout the sample, but typically nanoparticles with a diameter of 5–30 nm were observed (Figure 4). The larger particles correspond to superficial aggregation of the colloids during calcination.

Energy dispersive X-ray (EDX) analysis of these particles reveals the presence of Pd and Au in addition to the SiO_2 matrix material. The STEM–EDX line scan (Figure 5) shows that the nanoparticle consists of Pd and Au, which form a uniform alloy within the resolution limit of the EDX analysis. Quantification of the averaged line scan using the Pd-L and Au-L lines reveals a ratio of 48 wt % Au and 52 wt % Pd, which is within the accuracy of the EDX quantification, in good agreement with the nominal 50:50 alloy composition.

Cross-polarization magic-angle-spinning (CP/MAS) NMR spectroscopy: Figure 6 shows the ^{1}H-CP/MAS NMR spectrum of the D samples, 1 % Pd–Au/SiO_2. It contains the typical bands assigned to the NR_4^+ stabilizer (bands at 0.649, 1.348, and 7.664 ppm) and a band located at 2.820 ppm due to a −CH−O− group, a remnant from the solvent during the sol–gel synthesis. Heating the catalysts in hydrogen and air led to a different situation. Air-calcined catalysts produced materials in which no clear NMR band assigned to carbonaceous materials could be detected, while for the R series an advanced decomposition of the stabilizer template was indeed observed. The ^{13}C-CP/MAS NMR spectrum presented in Figure 7 for the R series, 1 % Pd–Au/SiO_2 catalyst demonstrates such behavior. The existence of the various carbon bonds in these catalysts seems indicative that the template was not completely removed.

The ^{29}Si CP/MAS NMR spectra of the the C series, 1 % Pd–SiO_2, 1 % Au–SiO_2, and 1 % Pd–Au/SiO_2 catalysts are given in Figure 8. These spectra show the characteristic structure for Si−O bonds. A ^{29}Si MAS analysis using the "block-decay" procedure indicated that the population of the Q^4 species slightly decreases for the Pd catalysts, which might be in line with the increased size of the Pd colloids. The differences between the R, C, and D series are very small. Although the Q^2 species were also detected, albeit at a low concentration, these data confirm a high degree of silica polymerization. With respect to the published data ,the Q^3/Q^4 ratio, compared with published data proved to be consistent with the incorporation of the colloids into the silica network.[83] On the basis of the same ^{29}Si MAS analysis it might be concluded that the so-called "T-surrounding species" are absent.

Catalytic tests, hydrogenation of styrene: Figure 9 shows the hydrogenation of styrene (Scheme 2) on the investigated catalysts. Samples D and E exhibited the highest activity in this reaction, which is in accordance with the exposed metallic surface. Calcining in air or even worse in hydrogen led to an important decrease of the activity (samples C and R).

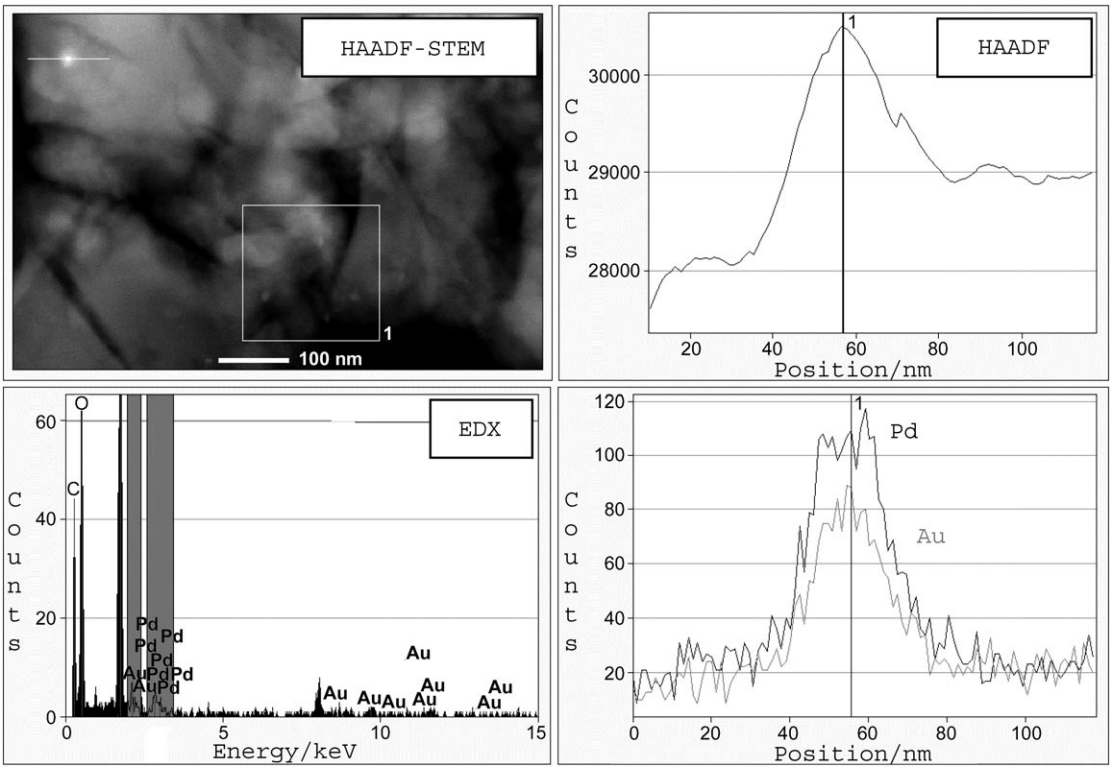

Figure 5. HAADF-STEM/EDX line profile showing the Au:Pd composition of a selected nanoparticle. Within the accuracy of the measurement, the composition does not change significantly throughout the particle.

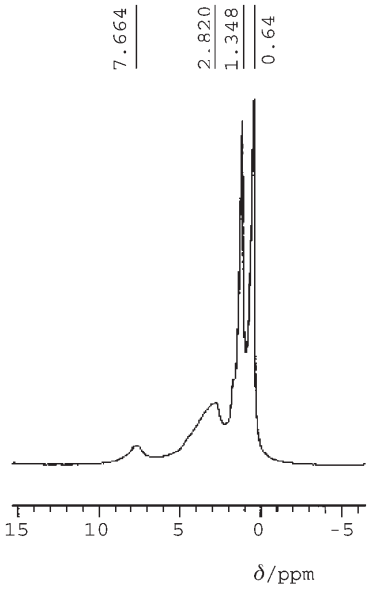

Figure 6. ^{1}H-CP/MAS NMR spectrum of D Pd–Au/SiO_2.

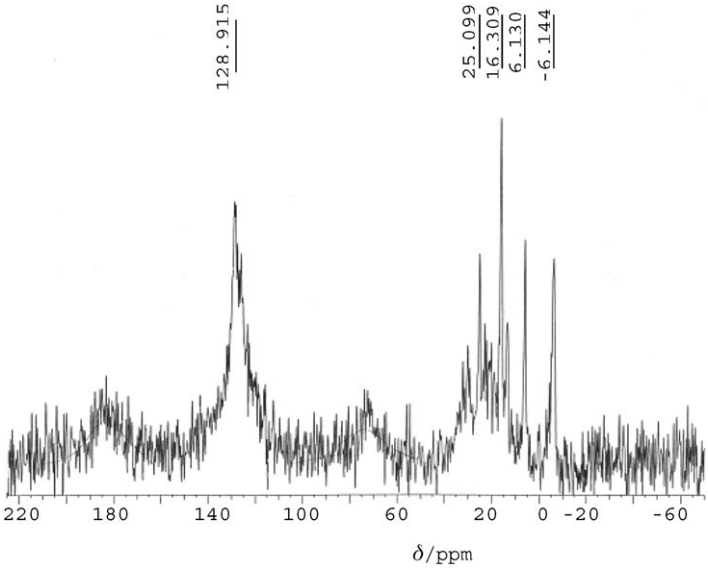

Figure 7. ^{13}C-CP/MAS NMR spectrum of R 1% Pd–Au/SiO_2.

The activity of samples D and E was very similar for all the investigated catalysts, indicating that for dried catalysts the presence of the stabilizers did not diminish the accessibility of the reactants. In both series, embedded Pd colloids exhibited higher activity than the Pd–Au alloys. Therefore, addition of Au in these catalysts leads to a decrease of the activity. The chemoselectivity was 100% to ethylbenzene for all of the catalysts investigated.

Hydrogenation of styrene in the presence of thiophene: Figure 10 shows variation of the activity for the hydrogenation of styrene in the presence of thiophene during several runs on the D catalysts. The poisoning with thiophene im-

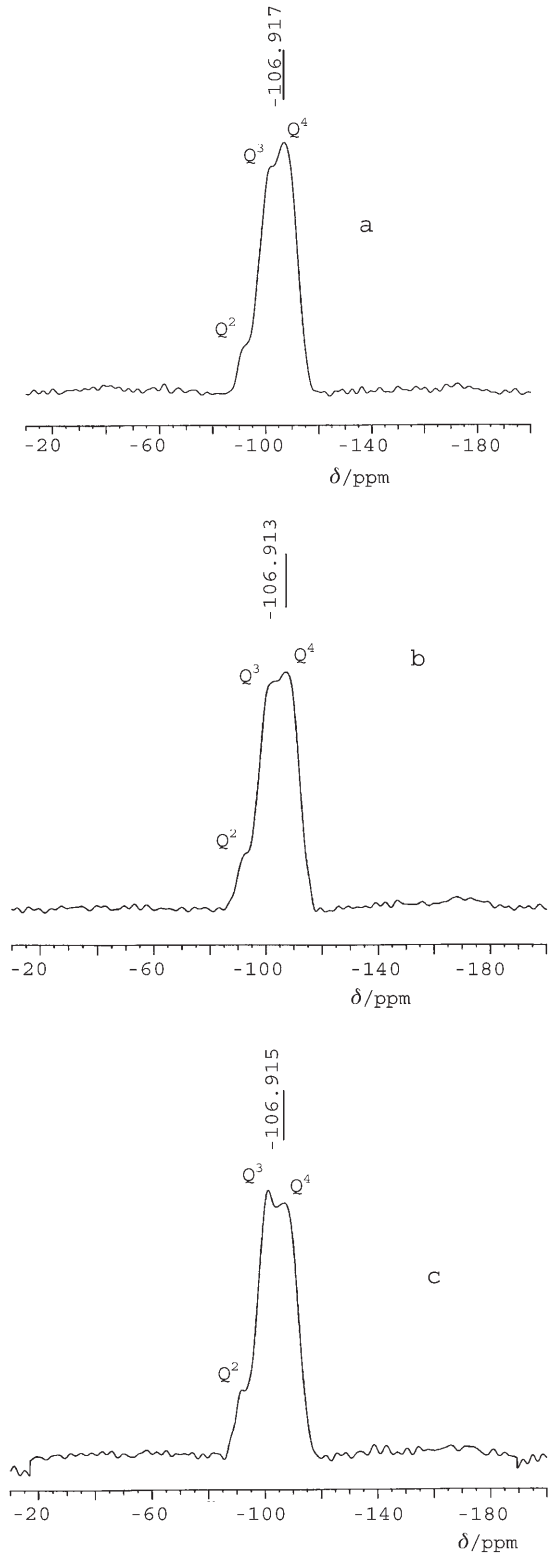

Figure 8. ^{29}Si CP/MAS NMR spectrum of a) C-1% Au-SiO_2 catalysts (Q^4:Q^3:Q^2=52:43:5), b) C-1% Pd–Au/SiO_2 (Q^4:Q^3:Q^2=51:42:7), and c) C-1% Pd-SiO_2 catalysts (Q^4:Q^3:Q^2=50:41:9).

pacted the activity of these catalysts differently; embedded Pd and Au colloids being much more dramatically affected than mixed Pd–Au colloids. After six runs, the activity of Pd catalysts approximated the activity of Pd–Au catalysts. It was thus observed that alloying of the two noble metals enhances the stability against poisoning with sulfur, which is indeed remarkable.

This behavior occurred irrespective of the way in which the catalysts were pretreated. Figure 11 shows variation of the activity in the presence of thiophene for the C catalyst series. In all the cases the poisoning with sulfur affected only the activity and not the selectivity.

Hydrogenation of 3-hexyn-1-ol: Figure 12 shows the behavior of the investigated catalysts in the hydrogenation of 3-hexyn-1-ol (Scheme 3). For the embedded colloids tested, the Pd–Au mixed colloids were the most effective, indicating the positive effect of alloying in this case. In terms of activity, the differences between the catalysts with 0.6 and 1.0 wt% were very small. The activity varied in the order E~D>C>R, which is in accordance with the accessibility to the metal surface.

The chemoselectivity towards hexenol reached 100% in the case of embedded Au colloids (Figure 13). The other catalysts also yielded hexenol and hexanol. However, even for these catalysts, the chemoselectivity to hexenol exceeded 95%. A remarkably high regioselectivity (*cis* selectivity >90%) was obtained for all catalysts. Again, the best results were obtained on Au and bimetallic Pd–Au catalysts, which exhibited a nearly complete *cis* selectivity. The addition of gold enhanced the regioselectivity relative to that of embedded Pd/SiO_2 colloids.

Hydrogenation of cinnamaldehyde: Figure 14 shows the variation of the activity in hydrogenation of cinnamaldehyde (Scheme 4) on catalysts with different pretreatments. These data refer to the transformation of cinnamaldehyde into cinnamyl alcohol, 3-phenylpropanal, and 3-phenyl-1-propanol. The activity of the investigated catalysts in this reaction was smaller, when compared to that determined for hydrogenation of 3-hexyn-1-ol or styrene. However, these data confirmed the results obtained in the hydrogenation of those molecules, with the D and E catalyst series being more active than the catalysts obtained at higher temperatures.

The selectivity to cinnamyl alcohol is the most important parameter in this reaction. Figures 15 and 16 present the variation of the selectivity for two series of catalysts, namely, C and D. These data correspond to a moderate selectivity in the desired product (ca. 50%). The way in which the catalysts were pretreated brought about only minor changes. On monometallic Pd- and Au-embedded colloids, 3-phenylpropanal and 3-phenyl-1-propanol were found to be the predominant reaction products. Alloying of the two nanometer-sized metals in colloids led to a very important enhancement of the selectivity, with respect to the monometallic ones, with cinnamyl alcohol being the major product.

The solvent plays a very important role in this reaction because the alcohols used leads to acetals. Thus, for the reactions carried out in ethanol, the formation of 1,1-dieth-

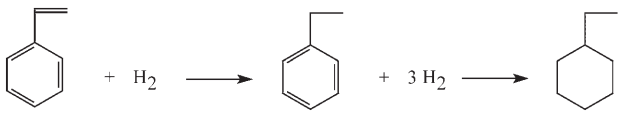

Scheme 2. Hydrogenation of styrene.

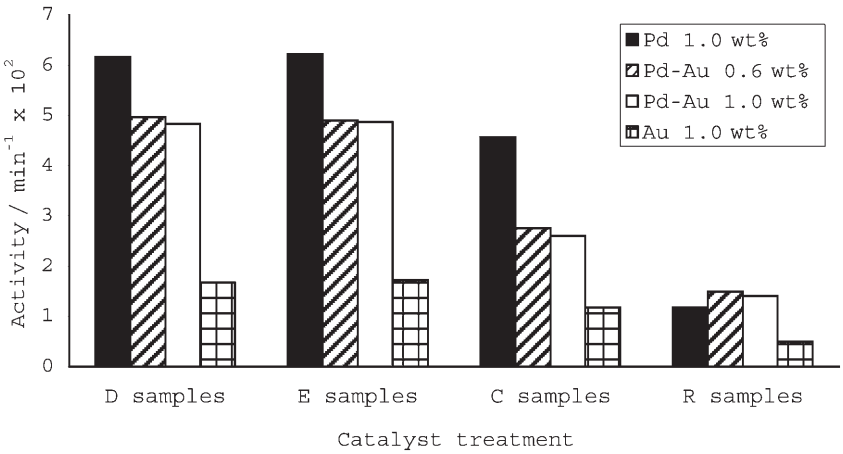

Figure 9. Comparative activity in the hydrogenation of styrene of the sol–gel embedded catalysts as a function of the pretreatment and colloid composition (10% conversion, 50 mg catalyst, 353 K, 20 bar H_2).

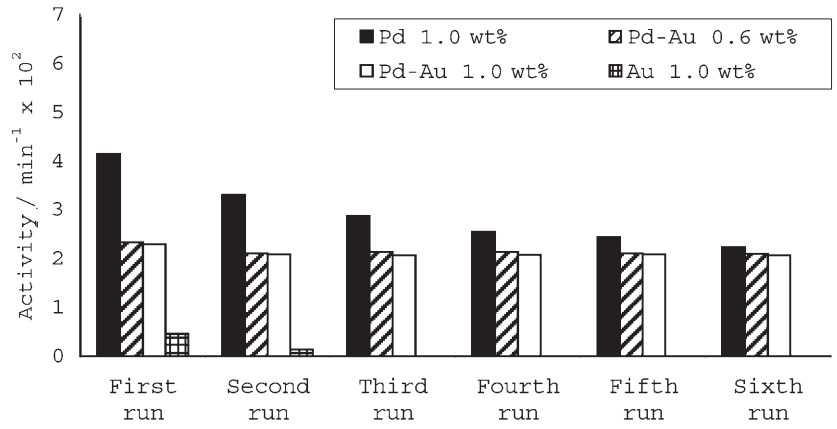

Figure 10. Evolution of activity for the D catalyst series in the presence of 100 ppm thiophene (50 mg catalyst, 353 K, 20 bar H_2, 30 min).

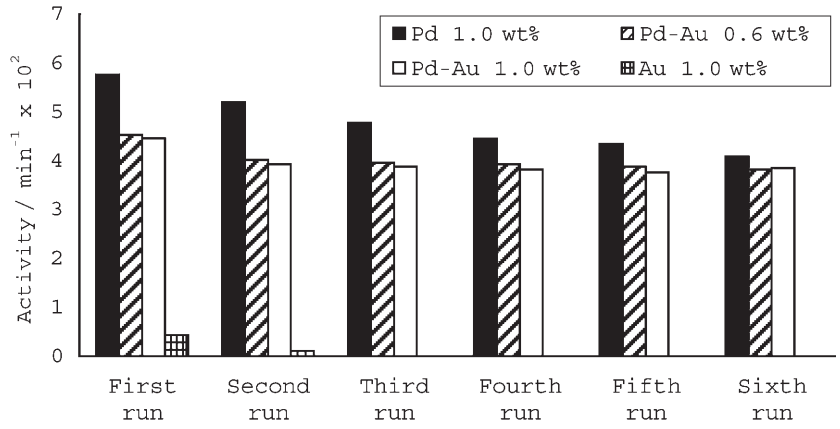

Figure 11. Evolution of the activity for the C catalyst series in the presence of 100 ppm thiophene (50 mg catalyst, 353 K, 20 bar H_2, 30 min).

oxy-3-phenylpropane occurred with conversions over 25%. It is worth noting that the conversion of cinnamaldehyde to 1,1-diethoxy-3-phenylpropane was even higher for embedded colloids than for pure silica, also prepared by means of the sol–gel route. In the presence of isopropanol as a solvent, the formation of acetals was less than 10%.

Discussion

Both Mössbauer and XRD analyses of the free Pd–Au colloid evidenced a fully alloyed material consisting of 52% Pd and 48% Au. These values correspond closely to those found by chemical and EDX analysis. Embedding of the Pd–Au colloids in the sol–gel matrix does not alter the Mössbauer spectrum. The similarities between the isomer shifts in the free Pd–Au colloid and in the embedded sample confirmed that no modification of the colloid structure had occurred during the sol–gel embedding process. The integrity of the incorporated Pd–Au alloy particles remained virtually untouched as evidenced by XPS. In addition, these measurements confirmed the preservation of the oxidation state irrespective of the treatment the catalysts were exposed to. No band assigned to any oxidized species has been detected in these analyses.

Preservation of the colloids was also confirmed by TEM analysis. TEM measurements (Figures 4 and 5) have confirmed a narrow size distribution of the incorporated, bimetallic colloid (about 5.0 nm).

Embedding of these colloids led to macroporous, solid materials with intermediate (ca. 300 $m^2 g^{-1}$) surface areas. The pore diameter and the porous texture could be associated with the characteristics of the surfactant used, that is, rather large stabilizers. SAXS has shown that the channels are randomly distributed and no

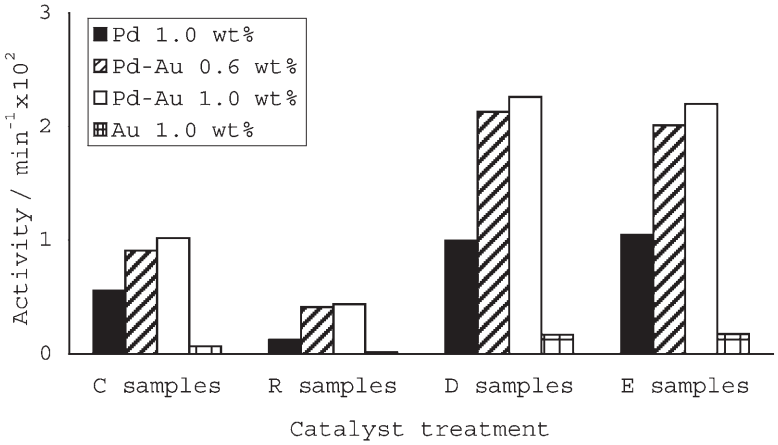

Figure 12. The activity in hydrogenation of 3-hexyn-1-ol of the catalysts differently pretreated (conversion 15%, 6.1 mL of 3-hexyn-1-ol, 50 mg of catalyst (1 wt-% metal incorporated), 20 bar H_2, 293 K).

hydrogen, the decomposition is not complete, as indicated from ^{13}C-CP/MAS NMR spectra. The surface areas of the R catalysts were low in comparison with the other catalysts, which may be an indication that the pores are partially blocked by coke deposits.

Alloying Pd with Au has long been expected to impart an improvement of the catalysts performances.[3–12] These results confirm that assumption. In addition, the uniformity of the metal-particle size in the cata-

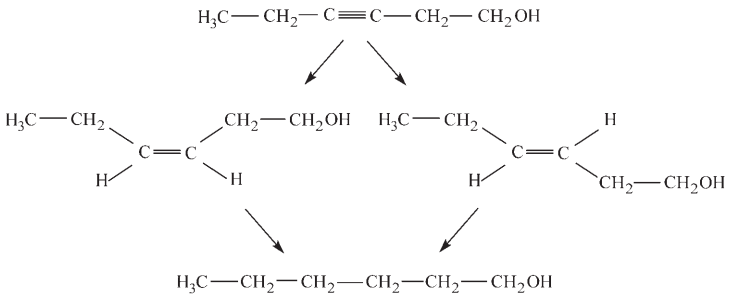

Scheme 3. Hydrogenation of 3-hexyn-1-ol.

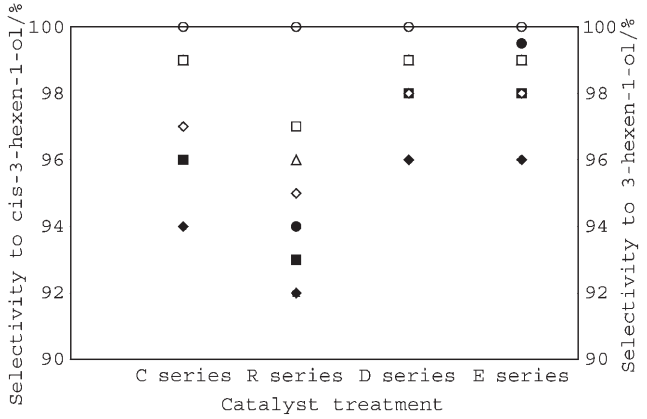

Figure 13. The chemoselectivity to 3-hexen-1-ol (◇,△,○,○) and regioselectivity for *cis*-3-hexen-1-ol (◆,▲,■,●) on the catalysts differently pretreated ((◇,◆-1%(Pd); △,▲- 0.6%(Pd); □,■- 1%(Pd-Au); ○,●-1%(Au); conversion 15%, 6.1 mL of 3-hexyn-1-ol, 50 mg of catalyst (1 wt% metal incorporated), 20 bar H_2, 293 K).

tubes (such as those found in MCM materials) or other organized pore architectures were present here. However, it is expected that around the colloids well-defined cavities exist (this is pretty speculative and should be verified by some scientific evidence).

CP/MAS NMR analysis indicated that the D series corresponded to catalysts in which the stabilizer compound is preserved without any damages. Silica is polymerized to a high degree in these catalysts, although by comparison with pure silica prepared by a sol–gel procedure, the content in the Q^3 species and the existence of Q^2 ones account for a lower degree of polymerization. Heating of these catalysts either in a hydrogen atmosphere or in air followed by reduction in hydrogen led to an expected decomposition of the stabilizer compounds. However, in the case of the catalysts treated directly in

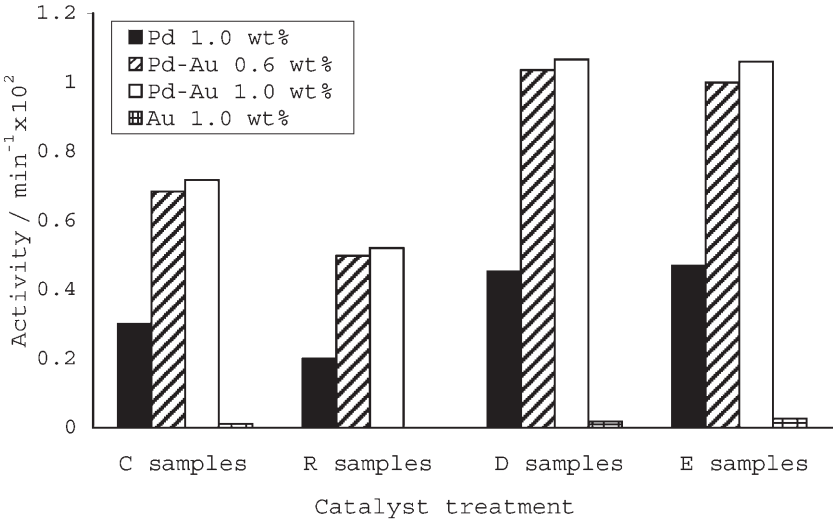

Figure 14. Variation of the activity as a function of the catalysts pretreatment (solvent isopropanol).

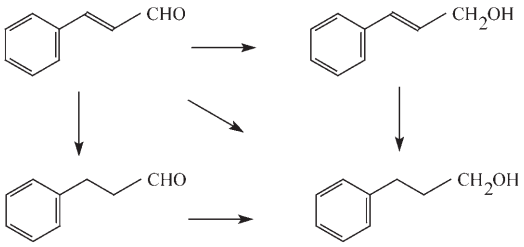

Scheme 4. Hydrogenation of cinnamaldehyde.

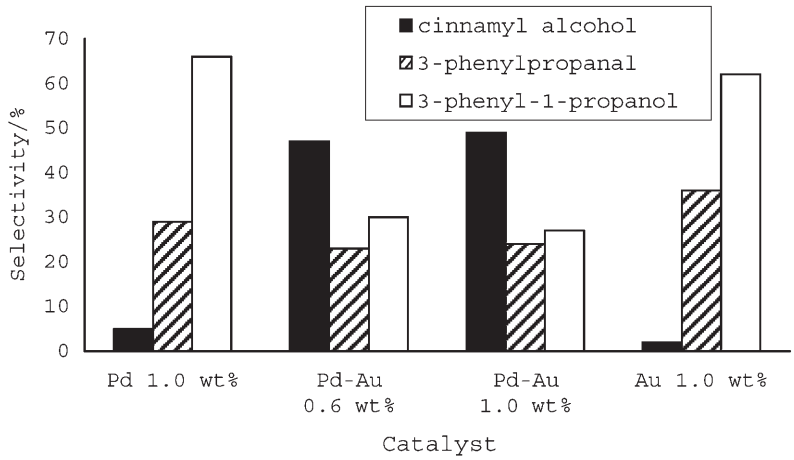

Figure 15. The variation of selectivity to cinnamalcohool, 3-phenylpropanal, and 3-phenyl-1-propanol for the C series of catalysts.

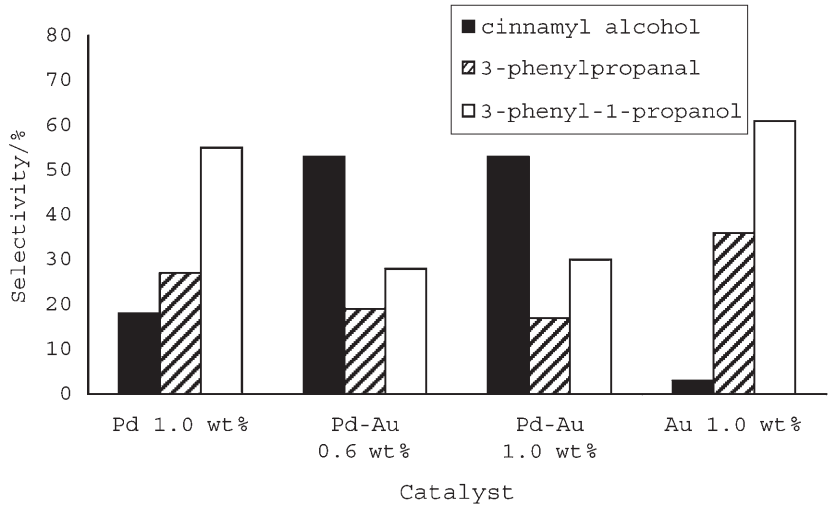

Figure 16. The variation of selectivity to cinnamyl alcohol, 3-phenylpropanal, and 3-phenyl-1-propanol for the D series of catalysts.

lysts prepared in this study eliminated any comment about the structure effects. The behavior of these catalysts in the investigated reactions differed according to the nature of the substrate molecule. However, since the activation of the catalysts imparts a strong influence on the performances of these catalysts only the results of the D series, which corresponds to the more active catalysts, will be discussed further. The results for the E series were very close to those for the D series, but the E series requires an additional step, that is, the extraction of the stabilizer ligand. The performances of the C and R series decreased in this order. These results may be explained, both by blocking of the pores by carbonaceous deposits (mostly in the case of the R series), but also by a blocking of the colloid surfaces by these deposits. The very good concordance of the activity of the catalysts with 1 and 0.6% (Pd–Au) confirmed the absence of any structure-sensitive effects.

Hydrogenation of pure styrene occurred with the higher activity on Pd colloids, while the addition of Au decreased the activity of the embedded colloids. Pure Au catalysts exhibited a very poor activity. However, reactions carried out in the presence of thiophene indicated that Pd–Au catalysts have a high level of tolerance to the poison, which might be of a great practical importance. It is not the case with Pd colloids, for which a continuous decrease of the activity in the presence of thiophene was observed. Hydrogenation of 3-hexyn-1-ol and cinnamaldehyde indicated Pd–Au colloids as the most active catalysts in the absence of any poison.

The selectivity of these catalysts is possibly more important in the investigated reactions. Hydrogenation of styrene occurred with a total chemoselectivity to ethylbenzene irrespective of the catalyst. No hydrogenation of the benzyl ring was detected. For the other molecules examined in hydrogenation reactions the chemical composition of the colloids was an important factor. Thus, in the hydrogenation of 3-hexyn-1-ol the interesting compound is *cis*-3-hexen-1-ol. Au colloids were the most chemoselective. The very high regioselectivity of these catalysts (*cis* selectivity $>90\%$) and the fact that bimetallic Pd–Au catalysts exhibited a near complete *cis* selectivity is also very important. These data clearly indicated that the addition of gold enhanced the regioselectivity, when compared with embedded Pd/SiO_2 colloids.

Hydrogenation of cinnamaldehyde represented the case in which a cooperative effect for these colloids was observed. As previously mentioned, the important product of this reaction is cinnamyl alcohol. Hydrogenation on both Pd and Au colloids led to a very poor selectivity for this compound. Alloying these metals into Pd–Au colloids resulted in an enhanced selectivity, when compared to the monometallic catalysts.

These data confirmed the fact that gold by itself, irrespective of the support (SiO_2, Al_2O_3, or MgO) exhibits a rather low catalytic hydrogenation activity.[13] However, recent studies demonstrated that nanometer-sized gold particles may act as active catalysts in selective hydrogenation of allylic compounds.[84–87] In the present study, although the size of gold particles was close to that reported by Claus et al.[84] both the activity and selectivity in the hydrogenation of cinnamaldehyde were very low. In this particular case, the addition to Pd was found to lead to an enhanced catalytic activity and selectivity, which might be interpreted in terms of electronic effects. In the case of hydrogenation of cinnamaldehyde and crotonaldehyde, the effect of the addition of a second metal such as Sn was interpreted as follows: the species created by tin in close proximity to the noble metal activate the C=O group.[88,89] A similar behavior can be expected in this case as well. Hydrogen-chemisorption data are also in line with these results.

Conclusion

The data presented in this paper show evidence that alloying of Pd with Au on a nanometer scale leads to improvements in activity in hydrogenation reactions and have a positive effect on the relevant chemoselectivity. The alloying of the two metals may improve catalyst tolerance to poisoning by sulfur compounds. The way in which the colloid-embedded catalysts were pretreated was crucial for the activity of these catalysts. High temperatures resulted in decomposition of the stabilizer ligand, which caused blockage of the colloid surface, and thus deactivation of the catalysts.

Experimental Section

Catalysts preparation: The Pd, Au, and Pd/Au (50% Au, 50% Pd) colloid precursors were prepared following a procedure described elsewhere.[70] Embedding of these colloids was carried out by using tetraethoxysilicate (TEOS) as the precursor for the silica support. Since the $NR_4C_8H_{19}$- stabilized Pd–Au colloids are completely insoluble and even decompose at elevated temperatures in alcoholic solutions, the normal sol–gel procedure required modification, thus THF was used as the solvent. To have comparable preparations, the same procedure was used for monometallic Pd and Au colloids. The molar composition of the sol was TEOS/THF/H_2O/HCl = 1:3.5:4:0.05 for the bimetallic Pd–Au and TEOS/THF/H_2O/HCl = 1:4.5:4:0.02 for Pd and Au monometallic systems. The above mixture was refluxed at 343 K for 2 d, after which the colloid was added as a 4.5 wt-% solution in THF for Pd–Au, 10.2 wt% solution in THF for Pd, and 8.4 wt% solution in THF for Au at room temperature. The gelation was carried out under vigorous stirring for 4 d. To avoid any decomposition in the presence of air, all steps were carried out under an Ar atmosphere. The resulting gel was dried at 383 K by using a ramp of 0.12 K min^{-1}. A portion of these materials was then calcined under air at 723 K with a ramp of 0.3 K min^{-1}. After cooling, the samples were reduced in a flow of pure hydrogen at 723 K using the same ramp. Reduction was carried out with a H_2 flow of 30 cm^3 min^{-1}. In some dried samples the surfactant was extracted using the procedure of Hitz and Prins.[77] Accordingly, the dried parent material (5 g) was stirred in an ethanol heptane azeotropic mixture (200 mL) for 1 h at 351 K, followed by filtration and washing.

In conclusion, four different routes were used to obtain the catalysts. The materials that were calcined in air and then reduced were denoted as C, those directly reduced in hydrogen as R, and those that were simply dried as D. Additionally, samples in which the surfactant was extracted using an ethanol heptane azeotropic mixture were denoted as E. Following these procedures bimetallic Pd–Au/SiO_2 catalysts with 0.6 and 1 wt% metal, and monometallic Pd and Au–SiO_2 catalysts with 1 wt% metal were prepared. The metal loading in these catalysts was confirmed by ICP–AES spectroscopy.

Catalysts characterization: Characterisation of the Pd–Au colloids, both in the free and in the embedded state, was first performed using TEM, EDX, and atomic absorption spectroscopy (AAS). In addition, nitrogen adsorption–desorption curves at 77 K, H_2-chemisorption measurements, solid-state ^{1}H, ^{13}C, and ^{29}Si-CP/MAS-NMR spectroscopy, XRD, SAXS, XPS, TEM, and ^{197}Au Mössbauer spectroscopy were applied.

The sorption isotherms of N_2 at 77 K were obtained with a Micromeritics ASAP 2000 apparatus after outgassing the samples at 393 K for 24 h under vacuum 0.00001 mbar.

H_2-chemisorption measurements were carried out using a Micromeritics ASAP 2010C apparatus. The samples were activated under vacuum at 403 K for 36 h. Afterwards, a hydrogen flow was passed initially at 308 K for 15 min, then the temperature was increased to 403 K at a heating rate of 5 K min^{-1} and maintained for 2 h. After reduction, the samples were purged with a helium flow at 403 K for 2 h and then at 308 K for another 30 min. The amount of chemisorbed hydrogen was measured at 308 K by the desorption method after equilibration for 45 min in 400 mbar of adsorbate. The total hydrogen uptake was determined by extrapolating the linear portion of the adsorption isotherm to zero pressure. Reversible H_2 sorption was measured by outgassing at 0.00005 mbar at the adsorption temperature and running a second isotherm. The difference between the total and reversible uptakes was ascribed to irreversible hydrogen uptake. The metal dispersion, surface area, and particle size were determined from the irreversible uptake, assuming a H/metal stoichiometry of 1. For the Pd–Au colloids, the calculation of dispersion was made considering Equations (1)–(3), in which V is the hydrogen uptake, SF is the calculated stoichiometry factor, weight$_i$ is the percentage of the sample weight, and A_m is the effective area of one active metal atom.

$$D = \frac{100\,\% \times 100\,\%}{22414} \times \frac{V \times \mathrm{SF}}{\frac{\%\mathrm{weightPd}}{W_{\mathrm{atomic}}\mathrm{Pd}} + \frac{\%\mathrm{weightAu}}{W_{\mathrm{atomic}}\mathrm{Au}}} \quad (1)$$

$$Ms = \frac{6.023 \times 10^{23}}{22412} \times V \times \mathrm{SF} \times A_m \quad (2)$$

$$Msm = Ms \times \frac{100\,\%}{\%\mathrm{weightPd} + \%\mathrm{weightAu}} \quad (3)$$

The XPS spectra were recorded by using a SSI X probe FISONS spectrometer (SSX-100/206) with monochromated $Al_{K\alpha}$ radiation. The spectrometer energy scale was calibrated using the Au4f$_{7/2}$ peak (binding energy 84.0 eV). For calculation of the binding energies, the C1s peak of the C-(C,H) component of adventitious carbon at 284.8 eV was used as an internal standard. To limit reoxidation, the reduced samples were transferred from the reduction setup to the XPS apparatus under isooctane. The peaks assigned to Pd3d$_{3/2}$, Au4d$_{3/2}$, Si2p, and O1s levels were analyzed.

XRD patterns were recorded with a D5000 Kristalloflex diffractometer from Siemens using $Cu_{K\alpha}$ radiation ($\lambda = 1.5418$ Å). Data acquisition was done in the $2\theta = 2$–$65°$ range, with a scan step of 0.03°.

SAXS experiments were performed with an evacuated Kratky compact camera mounted on a Siemens rotating copper anode. A take-off angle of 3° was used for these experiments. The power of the generator was set to 200 mA × 30 kV; selection of $Cu_{K\alpha}$ radiation was achieved with the help of a Ni filter, completed by electronic discrimination. A 1D proportional counter (mBraun OED50M) placed at a distance of 24.5 cm from the sample was used to record the scattering patterns. The channel width of the detector amounted to about 71 μm, close to the resolution of the detector. Precise values of channel width and sample-to-detector distances were obtained by measuring calibration standards, namely rat-tail collagen and crystalline monodisperse oligomers with the repeating unit (-F-O-F-O-F-CO-), in which F represents a *para*-linked aromatic moeity. The beam shape P(h,v) was measured in the plane of the detector in the horizontal direction with 0.658 cm as a standard deviation. In the vertical direction (v), the beam was very sharp (about 300 μm FWHM), and was thus considered as a delta function. The powders were introduced into Mark glass capillaries 1 mm in diameter. Acquisition times of 1800 s were used throughout. The scattering of an empty capillary was also recorded to obtain the so-called parasitic scattering. The parasitic scattering, scaled by sample transmittance, was subtracted from sample scattering to obtain the parasitic-corrected scattering.

The ^{197}Au Mössbauer measurements were performed with sources and absorbers cooled to 4.2 K in a liquid He bath cryostat. The sources were moved with a sinusoidal velocity waveform. An intrinsic Ge detector was used to detect the 77 keV gamma rays of ^{197}Au. The sources of ^{197}Pt ($T_{1/2} = 19$ h) were produced by irradiating isotopically enriched ^{196}Pt (ca. 200 mg) in a thermal neutron flux of about 2×10^{13} cm^2 s^{-1} at the Munich Research Reactor for about 20 h. For comparison with samples of Au–Pd colloids, a number of Au–Pd alloys of different compositions were prepared by arc melting in an argon atmosphere and subsequent rolling into foils of appropriate thickness. The Mössbauer spectra of all samples consisted of a single, more or less broadened line. To these experimental spectra, appropriate line shapes were fit by using transmission integral calculations.[90,91] It was found that line shapes corresponding to a Gaussian distribution of isomer shifts gave virtually perfect fits to the data. The emission line of the source and the distributed line width of the absorbers were assumed to be Lorentzian lines with a natural width of $\Gamma = 0.95$ mm s^{-1}.[92] Since the line broadening due to finite absorber thickness was taken into account by the transmission, integral fits, the variance σ of the Gaussian distribution of line positions in the absorbers is expected to be due only to the inhomogeneous line broadening in the alloy samples arising from the peculiar coordination and distribution of Au and Pd atoms in the vicinity of the Mössbauer atoms.

The MAS NMR experiments were performed at room temperature on a Bruker ASX100 spectrometer (2.33T) operating at a Larmor frequency of 19.89 MHz for ^{29}Si with a 4 mm probehead, and of 400.33 and 100.67 MHz with a 7 mm probehead for ^{1}H and ^{13}C, respectively. The MAS NMR spectra were obtained at 5 kHz spinning rate by using a single-pulse excitation ($\pi/10$). For ^{1}H spectra 32 transients were added with a recycling delay of 1 s. ^{13}C spectra were acquired with ^{1}H TPPM decoupling; 3000 scans were accumulated. ^{29}Si spectra were acquired with a 6 s recycle delay. ^{1}H and ^{13}C chemical shifts were referenced to TMS. The ^{29}Si chemical shifts were referenced relative to $Si(CH_3)_4$. The simulations were performed using the DMfit program.[93]

The electron microscopic analysis was performed by using a FEI Tecnai F20 ST instrument operating at 200 kV in STEM mode equipped with an EDAX r-TEM Si(Li) EDX detector with a super ultra-thin window (S-UTW). HAADF–STEM images and drift-corrected STEM–EDX line scans were acquired with a nominal spot size of 1 nm. The line scans were analyzed by using TIA software version 2.0.202. Quantification of the EDX spectra was done after background correction without thickness correction within TIA. The samples were prepared for TEM analysis by grinding the bulk material resulting in a fine powder, which was distributed on 200 mesh, carbon-coated copper grids.

Catalytic tests were carried out in selective hydrogenation of 3-hexyn-1-ol, which gives the corresponding *cis*-hexenol derivative (a valuable perfume ingredient),[46] of cinnamaldehyde to cinnamyl alcohol, which is used in the field of flavor and fragrances,[94] and of styrene, which is important for the treatment of the gasoline from pyrolysis.[95] Under standard test conditions, 3-hexyn-1-ol (6.1 mL) was converted without solvent in a stirred 50 mL stainless-steel autoclave using a catalyst (50 mg, 1 wt-% metal incorporated) at 20 bar hydrogen and 293 K. Experiments concerning hydrogenation of styrene were carried out in the same type of autoclave using the same volume of reactant and the same amount of catalyst at 20 bar hydrogen but at 353 K. Additionally, several runs were performed in which styrene (6.1 mL) and thiophene (100 ppm) were treated under similar experimental conditions. After each run, the catalyst was separated and reused in a new cycle. Hydrogenation of cinnamaldehyde was carried out in the same type of autoclave by using the substrate (1.1 mL) dissolved in ethanol or isopropanol (5 mL) under 20 bar hydrogen pressure and at 353 K. The reaction products were analysed by GC using a Varian Star 3400CX gas chromatograph equipped with a Chrompack 7530 capillary column (WCOT fused silica column with CP-Sil PONA CB stationary phase) and a Hewlett Packard 5890 series II gas chromatograph, using a WCOT Fused Silica CP-Wax 58 (FFAP) CB column, of 50 m length. The reaction products were identified using the same GC coupled with a Finnigan MAT SSQ7000 mass spectrometer and by ^{1}H and ^{13}C NMR spectroscopy with a Varian Gemini 300BB instrument, operating at 300 MHz for ^{1}H and 75 MHz for ^{13}C.

Acknowledgements

Vasile I. Pârvulescu thanks CERES, Project 4–140, and Ryan Richards thanks IUB for financial support.

[1] J. H. Sinfelt, G. H. Via, F. W. Lytle, *Catal. Rev. Sci. Eng.* **1984**, *26*, 81–140.
[2] G. C. Bond, *Chem. Soc. Rev.* **1991**, *20*, 441–475.
[3] J. P. Boitiaux, J. Cosyns, M. Derrien, G. Leger, *Hydrocarbon Process.* **1985**, *64*, 51–59.
[4] G. C. Bond, A. F. Rawle, *J. Mol. Catal. A* **1996**, *109*, 261–271.
[5] B. M. Chapnick, P. W. Paustian, E. Klainer, P. D. Joiner, A. L. Hyman, P. J. Kadowitz, UK Patent 1246015, **1971** to Bayer.
[6] G. Scarfe, W. Kronig, US Patent 3775342, **1973** to Bayer.
[7] P. Wirtz, K. Woerner, F. Wunder, K. Eichler, G. Roscher, European Patent 519436, **1992** to Hoechst.
[8] S. Hermans, M. Devillers, *Catal. Lett.* **2005**, *99*, 55–64.
[9] S. Morikawa, S. Samejima, M. Yositake, S. Tatsematsu, European Patent 0347830, **1989** for Asahi Glass Co.
[10] V. N. M. Rao, US Patent 5447896, **1995** to du Pont de Nemours. A. Malinowski.
[11] A. Malinowski, W. Juszczyk, J. Pielaszek, M. Bonarowska, M. Wojciechowska, Z. Karpinski, *Chem. Commun.* **1999**, 685–686.
[12] M. Nutt, J. Hughes, M. Wong, *Environ. Sci. Technol.* **2005**, *39*, 1346–1353.
[13] S. Galvagno, G. Parravano, *J. Catal.* **1979**, *57*, 272–286.
[14] J.-C. Legrand, A.-M. Diamy, G. Riahi, Z. Randriamanantenasoa, M. Polisset-Thfoin, J. Fraissard, *Catal. Today* **2004**, *89*, 177–182.
[15] S. Galvagno, G. Parravano, *J. Catal.* **1978**, *55*, 178–190.
[16] J. W. Sachtler, G. A. Somorjai, *J. Catal.* **1983**, *81*, 77–94.
[17] A. Sachdev, J. Schwank, *J. Catal.* **1989**, *120*, 353–369.
[18] N. Toshima, M. Harada, Y. Yamazaki, K. Asakura, *J. Phys. Chem.* **1992**, *96*, 9927–9933.
[19] H. Liu, G. Mao, M. Meng, *J. Mol. Catal.* **1992**, *74*, 275–284.
[20] M. Harada, K. Asakura, N. Toshima, *J. Phys. Chem.* **1993**, *97*, 5103–5114.
[21] Y. Mizukoshi, T. Fujimoto, Y. Nagata, R. Oshima, Y. Maeda, *J. Phys. Chem. B* **2000**, *104*, 6028–6032.

[22] H. Remita, A. Etcheberry, J. Belloni, *J. Phys. Chem. B* **2003**, *107*, 31–36.
[23] R. Harpeness, A. Gedanken, *Langmuir* **2004**, *20*, 3431–3434.
[24] M. L. Wu, D. H. Chen, T. C. Huang, *Langmuir* **2001**, *17*, 3877–3883.
[25] M. Bonarowska, J. Pielaszek, W. Juszczyk, Z. Karpinski, *J. Catal.* **2000**, *195*, 304–315.
[26] E. L. Kugler, M. Boudart, *J. Catal.* **1979**, *59*, 201–210.
[27] W. Juszczyk, Z. Karpinski, J. Pielaszek, Z. Paal, *J. Catal.* **1993**, *143*, 583–593.
[28] W. Juszczyk, Z. Karpinski, D. Lomot, J. Pielaszek, J. W. Sobczak, *J. Catal.* **1995**, *151*, 67–76.
[29] R. J. Wu, T. Y. Chou, C. T. Yeh, *Appl. Catal. B* **1995**, *6*, 105–116.
[30] Z. Karpinski, *Adv. Catal.* **1991**, *37*, 45–100.
[31] A. Malinowski, W. Juszczyk, D. Lomot, J. Pielaszek, Z. Karpinski, *Polish. J. Chem.* **1995**, *69*, 308–315.
[32] M. Boudart, G. Meitzner, in *EXAFS and Near Edge Structure III* (Eds.: K. O. Hodgson, B. Hedman, J. E. Penner-Halm), Springer, Berlin, **1984**, p. 217.
[33] A.-M. Diamy, Z. Randriamanantenasoa, J.-C. Legrand, M. Polisset-Thfoin, J. Fraissard, *Chem. Phys. Lett.* **1997**, *269*, 327–332.
[34] R. J. Davis, M. Boudart, *J. Phys. Chem.* **1994**, *98*, 5471–5477.
[35] S. H. Inami, H. Wise, *J. Catal.* **1972**, *26*, 92–96.
[36] L. Guczi, A. Beck, A. Horváth, Zs. Koppány, G. Stefler, K. Frey, I. Sajó, O. Geszti, D. Bazin, J. Lynch, *J. Mol. Catal. A* **2003**, *204/205*, 545–552.
[37] A. M. Venezia, L. F. Liotta, G. Pantaleo, V. La Parola, G. Deganello, A. Beck, Zs. Koppány, K. Frey, D. Horváth, L. Guczi, *Appl. Catal. A* **2003**, *251*, 359–368.
[38] J. W. Couves, P. Meeham, *Phys. B* **1995**, *208–209*, 665–667.
[39] J. Turkevich, G. Kim, *Science* **1970**, *169*, 873–879.
[40] *New Horizons in Catalysis*: R. S. Miner, Jr., S. Namba, J. Turkevich, *Stud. Surf. Sci. Catal.* **1981**, *7*, 160–167.
[41] G. Schmid, A. Lehnert, J.-O. Malm, J.-O. Bovin, *Angew. Chem.* **1991**, *103*, 852–854; *Angew. Chem. Int. Ed. Engl.* **1991**, *8*, 1015–1016.
[42] M. Harada, K. Asakura, N. Toshima, *J. Phys. Chem.* **1993**, *97*, 5103–5114.
[43] N. Toshima, *Fine Particles Science and Technology* (Ed.: E.Pelizzetti), Kluwer Academic, **1996**, p. 371.
[44] Y. Mizukoshi, K. Okitsu, Y. Maeda, T. A. Yamamoto, R. Oshima, Y. Nagota, *J. Phys. Chem.B* **1997**, *101*, 7033–7037.
[45] G. Schmid, H. West, H. Mehles, A. Lehnert, *Inorg. Chem.* **1997**, *36*, 891–895.
[46] H. Bönnemann, W. Brijoux, A. Schulze Tilling, K. Siepen, *Top. Catal.* **1998**, *4*, 217–227.
[47] H. Bönnemann, W. Brijoux, *Advanced Catalysts and Nanostructured Materials* (Ed.: W. R. Moser), Academic Press, San Diego, **1996**, p. 165.
[48] H. Bönnemann, R. Brinkmann, W. Brijoux, E. Dinjus, T. Joussen, B. Korall, *Angew. Chem.* **1991**, *103*, 1344–1346; *Angew. Chem. Int. Ed. Engl.* **1991**, *10*, 1312–1314.
[49] *Preparation of Catalysts IV*: J. B. Michel, J. T. Schwartz, *Stud. Surf. Sci Catal.* **1987**, *31*, 669–678.
[50] Y. Nakamura, H. Hirai, *Chem. Lett.* **1986**, 1197–1200.
[51] H. Hirai, M. Ohtaki, M. Komiyama, *Chem. Lett.* **1986**, 269–272.
[52] Y. Nakao, K. Kaeriyama, *J. Colloid Interface Sci.* **1989**, *131*, 186–191.
[53] Y. Wang, H. Liu, Y. Huang, *Polym. Adv. Technol.* **1996**, *7*, 634–639.
[54] Q. Wang, H. Liu, Y. Wang, *J. Colloid Interface Sci.* **1997**, *190*, 380–386.
[55] Y. Wang, H. Liu, Y. Y. Jiang, *Chem. Commun.* **1998**, 1878–1879.
[56] W. Yu, M. Liu, H. Liu, X. An, Z. Liu, X. Ma, *J. Mol. Catal. A* **1999**, *142*, 201–211.
[57] B. Corain, K. Jerabek, P. Centomo, P. Canton, *Angew. Chem.* **2004**, *116*, 977–980; *Angew. Chem. Int. Ed.* **2004**, *43*, 959–962.
[58] B. Corain, C. Burato, P. Centomo, S. Lora, W. Meyer-Zaika, G. Schmid, *J. Mol. Catal. A* **2005**, *225*, 189–195.
[59] R. W. J. Scott, A. K. Datye, R. M. Crooks, *J. Am. Chem. Soc.* **2003**, *125*, 3708–3709.
[60] R. W. J. Scott, O. M. Wilson, S.-K. Oh, E. A. Kenik, R. M. Crooks, *J. Am. Chem. Soc.* **2004**, *126*, 15583–15591.
[61] G. Ihlein, B. Junges, U. Jungas, F. Laeri, F. Schüth, U. Vietze, *Appl. Organomet. Chem.* **1998**, *12*, 305–314.
[62] M. T. Reetz, M. Dugal, *Catal. Lett.* **1999**, *58*, 207–212.
[63] S. Tao, Z. Zhan, G. Meng, *J. Mater. Sci. Lett.* **1999**, *18*, 707–710.
[64] E. Lindner, T. Schneller, F. Auer, H. A. Mayer, *Angew. Chem.* **1999**, *111*, 2288–2309; *Angew. Chem. Int. Ed.* **1999**, *38*, 2155–2174.
[65] F. Schweyer, P. Braunstein, C. Estournes, J. Guille, H. Kessler, J.-L. Paillaud, J. Rose, *Chem. Commun.* **2000**, 1271–1272.
[66] P. Braunstein, R. Devenish, P. Gallezot, B. T. Heaton, C. J. Humphreys, J. Kervennal, S. Mulley, M. Ries, *Angew. Chem.* **1988**, *100*, 972–973; Angew. Chem. Int. Ed. Engl. **1988**, 27, 927–929.
[67] K. M. K. Yu, C. M. Y. Yeung, D. Thompsett, S. C. Tsang, *J. Phys. Chem. B* **2003**, *107*, 4515–4526.
[68] R. W. J. Scott, C. Sivadinarayana, O. M. Wilson, Z. Yan, D. W. Goodman, R. M. Crooks, *J. Am. Chem. Soc.* **2005**, *127*, 1380–1381.
[69] S. Mandal, D. Roy, R. V. Chaudhari, M. Sastry, *Chem. Mater.* **2004**, *16*, 3714–3724.
[70] H. Bönnemann, U. Endruschat, B. Tesche, A. Rufínska, C. W. Lehmann, F. E. Wagner, G. Filoti, V. Pârvulescu, V. I. Pârvulescu, *Eur. J. Inorg. Chem.* **2000**, 819–822.
[71] M. Sasaki, M. Osada, N. Sugimoto, S. Inagaki, Y. Fukushima, A. Fukuoka, M. Ichikawa, *Microporous Mesoporous Mater.* **1998**, *21*, 597–606.
[72] M. Ichikawa, in *Metal Clusters in Chemistry* (Eds.: P. Braunstein, L. A. Oro, P. R. Raithby), Wiley-VCH, Weinheim, **1999**, p. 1273.
[73] A. Fukuoka, H. Araki, Y. Sakamoto, S. Inagaki, Y. Fukushima, M. Ichikawa, *Inorg. Chim. Acta* **2003**, *350*, 371–378.
[74] T. Hanaoka, H.-P. Kormann, M. Kroll, T. Sawitowski, G. Schmid, *Eur. J. Inorg. Chem.* **1998**, 807–812.
[75] T. Hanaoka, A. Heilmann, M. Kroll, H.-P. Kormann, T. Sawitowski, G. Schmid, P. Jutzi, A. Klipp, U. Kreibig, R. Neuendorf, *Appl. Organomet. Chem.* **1998**, *12*, 367–373.
[76] P. Braunstein, H.-P. Kormann, W. Meyer-Zaika, R. Pugin, G. Schmid, *Chem. Eur. J.* **2000**, *6*, 4637–4646.
[77] S. Hitz, R. Prins, *J. Catal.* **1997**, *168*, 194–206.
[78] Y. I. Lam, M. Boudart, *J. Catal.* **1977**, *50*, 530–540.
[79] M. P. A. Viegers, J. M. Trooster, *Phys. Rev. B* **1977**, *15*, 72–83.
[80] L. Steviano, S. Santucci, L. Lozzi, S. Colagero, F. E. Wagner, *J. Non-Cryst. Solids* **1998**, *232–234*, 644–649.
[81] J. M. Tura, P. Regull, L. Victori, M. Dolors de Castellar, *Surf. Interface Anal.* **1988**, *11*, 447–449.
[82] N. H. Turner, A. M. Single, *Surf. Interface Anal.* **1990**, *15*, 215–222.
[83] J. T. Payne, D. A. Reuschle, K. A. Mauritz, *Polym. Prepr.* **1997**, *38*, 247–248.
[84] P. Claus, A. Bruckner, C. Mohr, H. Hofmeister, *J. Am. Chem. Soc.* **2000**, *122*, 11430–11439.
[85] C. Mohr, H. Hofmeister, P. Claus, *J. Catal.* **2003**, *213*, 86–94.
[86] J. E. Bailie, G. J. Hutchings, *Chem. Commun.* **1999**, 2151–2152.
[87] C. Milone, R. Ingoglia, M. L. Tropeano, G. Neri, S. Galvagno, *Chem. Commun.* **2003**, 868–869.
[88] J. L. Margitfalvi, A. Tompos, I. Kolosova, J. Valyon, *J. Catal.* **1998**, *174*, 246–249.
[89] P. Gallezot, D. Richard, *Catal. Rev. Sci. Eng.* **1998**, *40*, 81–126.
[90] G. Lang, Nucl. *Instr. Methods* **1963**, *24*, 425–431.
[91] T. E. Cranshaw, *J. Phys. E* **1974**, *7*, 497–505.
[92] G. K. Shenoy, B. D. Dunlap, *Mossbauer Isomer Shifts* (Eds.: G. K. Shenoy, F. E. Wagner), North Holland, Amsterdam, **1978**, p. 869.
[93] D. Massiot, F. Fayon, M. Capron, I. King, S. Le Calvé, B. Alonso, J. O. Durand, B. Bujoli, Z. Gan, G. Hoatson, *Magn. Reson. Chem.* **2002**, *40*, 70–76.
[94] V. I. Parvulescu, V. Parvulescu, S. Kaliaguine, U. Endrushat, B. Tesche, H. Bonnemann, in *Catalysis of Organic Reactions* (Ed.: M. E. Ford), Marcel Dekker, **2001**, p. 301.
[95] V. I. Pârvulescu, V. Pârvulescu, D. Macovei, L. Frunza, *J. Chem. Soc. Faraday Trans.* **1997**, *93*, 1827–1835.

Received: August 9, 2005
Published online: December 27, 2005

